Single-molecule detection of structural changes during Per-Arnt-Sim (PAS) domain activation

Jason Ming Zhao[†‡§], Haeshin Lee[¶‖], Rene A. Nome[‡††], Sophia Majid[¶], Norbert F. Scherer[‡††], and Wouter D. Hoff[¶‡‡]

Departments of [†]Physics, [¶]Biochemistry and Molecular Biology, and [††]Chemistry and [‡]Institute for Biophysical Dynamics, University of Chicago, Chicago, IL 60637

Edited by Robert H. Austin, Princeton University, Princeton, NJ, and approved June 12, 2006 (received for review February 24, 2006)

The Per-Arnt-Sim (PAS) domain is a ubiquitous protein module with a common three-dimensional fold involved in a wide range of regulatory and sensory functions in all domains of life. The activation of these functions is thought to involve partial unfolding of N- or C-terminal helices attached to the PAS domain. Here we use atomic force microscopy to probe receptor activation in single molecules of photoactive yellow protein (PYP), a prototype of the PAS domain family. Mechanical unfolding of Cys-linked PYP multimers in the presence and absence of illumination reveals that, in contrast to previous studies, the PAS domain itself is extended by ≈3 nm (at the 10-pN detection limit of the measurement) and destabilized by ≈30% in the light-activated state of PYP. Comparative measurements and steered molecular dynamics simulations of two double-Cys PYP mutants that probe different regions of the PAS domain quantify the anisotropy in stability and changes in local structure, thereby demonstrating the partial unfolding of their PAS domain upon activation. These results establish a generally applicable single-molecule approach for mapping functional conformational changes to selected regions of a protein. In addition, the results have profound implications for the molecular mechanism of PAS domain activation and indicate that stimulus-induced partial protein unfolding can be used as a signaling mechanism.

atomic force spectroscopy | photoactive yellow protein | receptor activation

Biological signaling starts with the activation of receptor proteins, in which stimuli trigger protein conformational changes that relay a signal to an associated signal transduction chain. A central question concerns the nature of the structural changes that activate a receptor protein. The mechanism of signaling by Per-Arnt-Sim (PAS) domain-containing proteins is of considerable interest, because these structural domains occur in many signaling proteins (1). In addition, incorrect signaling by PAS domains is associated with a range of diseases. Important examples are mutations in the human ERG potassium channel, which causes cardiac arrhythmias (2), and the involvement of hypoxia-inducible factors in myocardial and cerebral ischemia (3).

We investigate the photoinduced structural changes in the bacterial blue light receptor, photoactive yellow protein (PYP), a prototype for PAS domains (4). As shown in Fig. 1, PYP consists of two N-terminal α-helices (residues 1–25), followed by a typical PAS domain (1, 5) fold (residues 26–125) that contains a central six-stranded β-sheet flanked by α-helices (6). The protein exhibits photochemistry based on its *p*-coumaric acid chromophore (7). Blue light converts the initial pG state of PYP into the photoactivated pB state in milliseconds, whereas pB decays back to pG in ≈0.5 s (8). The pB state is believed to trigger negative phototaxis in purple bacteria (9).

The structural changes that occur upon pB formation involve partial unfolding of the receptor, indicating partial protein unfolding as a novel signaling mechanism (10). Although the crystal structure of a pB-like state exists (11), Xie *et al.* (12) have shown that the motion of PYP is greatly hindered in a protein crystal. Thus, the degree to which different regions of PYP unfold in solution upon pB formation remains an open question. Previous solution spectroscopy experiments indicate that unfolding of the two N-terminal helices of PYP is involved (10, 13–15). Recent NMR measurements on a PYP mutant lacking the 25 N-terminal residues indicate that regions outside the central β-sheet also undergo a significant increase in flexibility (16). Interestingly, activation of LOV, a PAS domain blue-light receptor in plants, involves partial unfolding of a C-terminal helix immediately beyond the PAS domain core of the receptor (17), suggesting that the unfolding of N- or C-terminal helices is a general theme in PAS domain activation. Here, we use single-molecule force microscopy to probe the axis-dependent stability and structural changes in the PAS domain core of PYP that occur upon photoactivation.

Single-molecule pulling experiments involve the concomitant measurement of the distance between two attachment points and the force needed to extend the molecule (18–20). If the attachment points for pulling are well defined, such measurements intrinsically combine structural and energetic information. We used this approach to probe conformational changes in selected regions of PYP upon its activation.

A pair of surface-exposed residues were mutated to Cys, and the resulting PYP mutants were linked into a linear chain (polyPYP) via disulfide bonds to allow measurements of the distance between the two amino acid residues (see *Materials and Methods*). Similar chemical-linking strategies have recently been reported in studies of polyGFP by Dietz *et al.* (21), polyubiquitin by Carrion-Vazques *et al.* (20), polyE2lip3 (an all-β protein) by Brockwell *et al.* (22), and polylysozyme by Yang *et al.* (23). Single polyPYP assemblies were stretched by using an atomic force microscope (AFM) to measure the unfolding length (ΔL) and unfolding force (ΔF) for individual PYP molecules. When an external force is applied to the ends of the polyPYP chain, each PYP molecule experiences a force distributed across the region of the protein located between the two Cys side chains. Thus, the choice of the positions of the Cys mutations defines the orientation of the force vector across individual proteins and localizes the region of the protein to which the force-extension measurement is sensitive. The initial position of the two Cys residues is known from the crystal structure, and the experimental results report changes in the distance and force between the two Cys residues along this well defined coordinate.

Conflict of interest statement: No conflicts declared.

This paper was submitted directly (Track II) to the PNAS office.

Abbreviations: PAS, Per-Arnt-Sim; PYP, photoactive yellow protein; MD, molecular dynamics; SMD, steered MD.

[§]Present address: Department of Radiology, Johns Hopkins University, Baltimore, MD 21205.

[‖]Present address: Department of Biomedical Engineering, Northwestern University, Evanston, IL 60208.

[‡‡]To whom correspondence should be sent at the present address: Department of Microbiology and Molecular Genetics, Oklahoma State University, Stillwater, OK 74078. E-mail: wouter.hoff@okstate.edu.

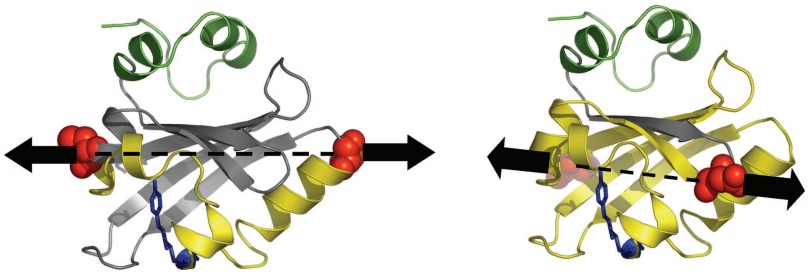

Fig. 1. Cys-directed PYP double mutants for multimerization. A pair of surface-exposed residues (in red) in wild-type PYP (Protein Data Bank ID code 2PHY) were mutated to Cys: residues 48/85 (*Left*) and residues 36/128 (*Right*). The doubly mutated PYP spontaneously multimerizes via disulfide bonds under oxidizing conditions. The protein region (in yellow) between the two Cys mutations is stretched in the AFM experiments. The two axes defined by the residue pairs 48/85 and 36/128 are indicated by dashed lines. The N-terminal domain is shown in green.

Results and Discussion

Biochemical Construction of polyPYP. Two PYP double mutants were constructed with Cys mutations at residues 36/128 and residues 48/85 (Fig. 1). These positions were chosen to examine the unresolved extent of the light-induced structural changes in the PAS domain core of PYP. The photochemistry and photocycle dynamics of these mutants is indistinguishable from native PYP (see the supporting information, which is published on the PNAS web site). The 36/128 mutant, which involves an Ala–Ala–Cys extension at the C terminus to facilitate the Cys-directed multimerization reaction, is designed to probe structural and stability changes in the whole PAS domain upon activation, whereas the 48/85 mutant focuses on the corresponding changes around the chromophore of the PAS domain (designated as PAS–Chr), i.e., the 37 aa flanking the chromophore attached to Cys-69. The two vectors defined by the 36/128 and 48/85 Cys pairs both pass near the protein's center of mass, and are at a 60° angle with respect to each other in nearly the same plane, as deduced from the x-ray structure of PYP (6).

The multimerization of the 48/85 mutant of PYP was analyzed by SDS/PAGE and MALDI-TOF MS, revealing that the resulting samples contained polyPYP with >10 subunits (Fig. 2). The disulfide-linking reaction occurred spontaneously in solution in the presence of air. PolyPYP with 10 subunits formed readily in 8 h. The specificity of the linkage is defined by the positions of Cys mutations on the PYP. The PYP orientations can be parallel or antiparallel relative to each other, but this is unlikely to have a significant effect on the force extension properties of the polyPYP molecule. The simple solution biochemistry and the specificity of the multimerization reaction make this technique easily generalizable to other proteins, offering a powerful tool for axis-dependent, single-molecule experiments. The multimerization reaction of the 36/128 PYP mutant yielded similar results, although the maximum size of this polyprotein was usually in the range of 6–8.

Force–Extension Curves in the Dark and Under Illumination. Representative force–distance curves (Fig. 3) measured for polyPYP in the dark (Fig. 3, black curves) and under saturating (supporting information) continuous blue light illumination (Fig. 3, blue curves) show a characteristic sawtooth pattern of protein ruptures (19, 20, 24). The distance between dips and the height of each peak represent ΔL and ΔF, respectively, for the unfolding of the PAS or PAS–Chr regions of PYP into an extended amino acid chain. The data show that photoexcitation reduces both the extensible length, ΔL, and mechanical stability, ΔF, of these two regions in PYP. These structural changes are reversible. Inter-

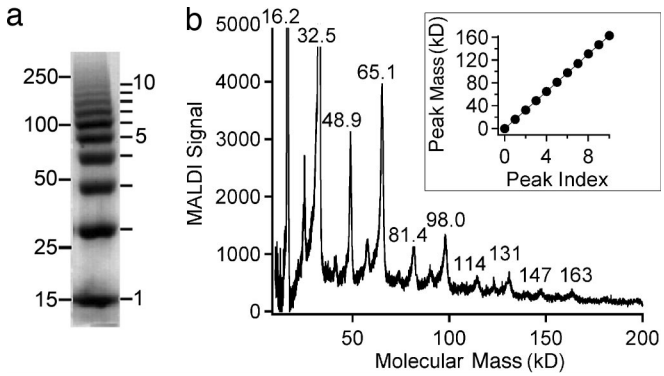

Fig. 2. Analysis of the multimerization state of 48/85 PYP. SDS/PAGE gel electrophoresis (*a*) and MALDI-TOF MS (*b*) of polyPYP show distinct species whose molecular masses are integer multiples of the monomer molecular mass. The bars in *a* are the molecular masses of the molecular mass markers on the left and the multimeric state of the PYP sample on the right. (*b*) The *Inset* shows the MALDI-TOF peak mass values vs. the peak number. A linear fit yields a slope equal to 16.3 kDa, corresponding to the molecular mass of a PYP monomer.

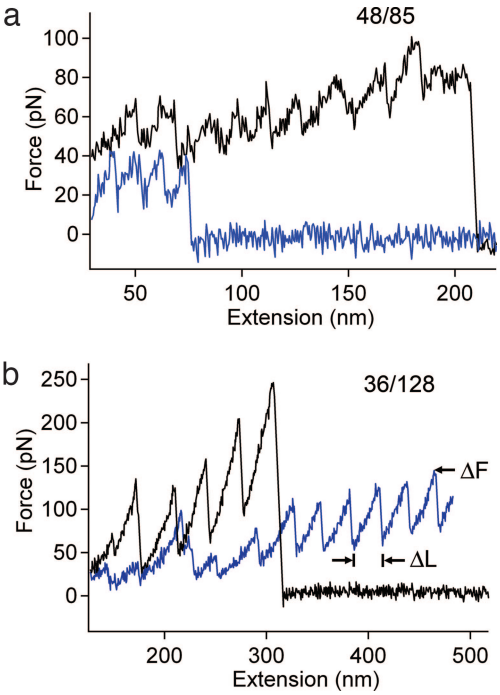

Fig. 3. AFM force vs. distance curves (pulling rate 1 μm/s) for the unfolding of single polyPYP molecules along the 48/85 axis (*a*) and the 36/128 axis (*b*) in the dark (in black) and during continuous blue light illumination (in blue).

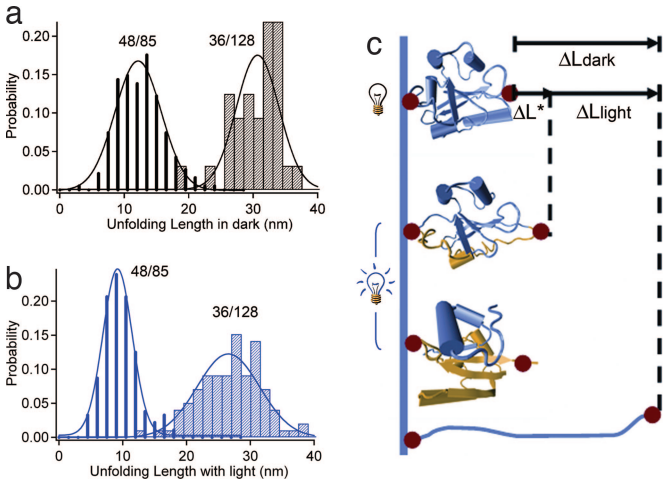

Fig. 4. Changes in local structure during light activation of single PYP molecules. (*a* and *b*) Unfolding length distributions of 36/128 (hatched bars) and 48/85 (solid bars) PYP in the dark (black, *a*) and under continuous illumination (blue, *b*). The pulling rates were 5 μm/s and 1 μm/s for the 36/128 and 48/85 mutants, respectively. (*c*) The unfolding length ΔL measures the length gain when the sequence (in yellow) between the two Cys mutations of a folded PYP (top structure) is mechanically unfolded into an extended amino acid chain (bottom structure, schematic). The two middle structures are schematic representations of PYP in the photoactivated pB state along two pulling axes. The difference in the unfolding lengths in the dark and under illumination, ΔL^*, is a measure of the local structural change in the selected region of PYP due to light activation.

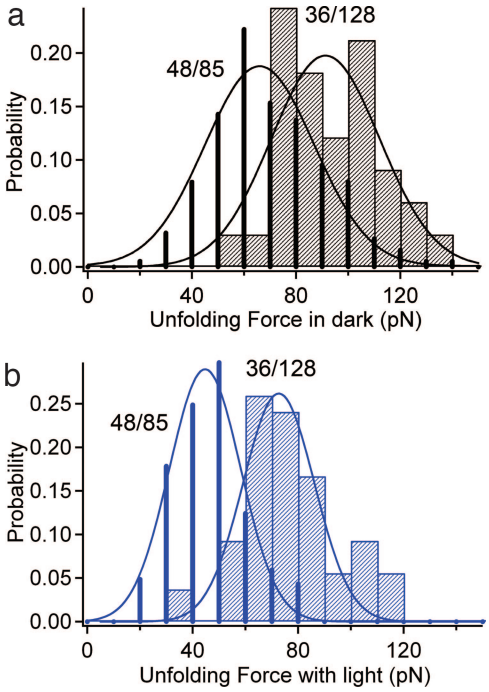

Fig. 5. Anisotropy and light-induced changes in the global stability of PYP probed by mechanical unfolding along two different axes. Unfolding force distributions of 36/128 (hatched bars) and 48/85 (solid bars) PYP in the dark (black, *a*) and under illumination (blue, *b*). The pulling rate was 1 μm/s.

ruption of the illumination allows the PYP modules to relax to the dark state, and the original force and length distributions are recovered (supporting information). This recovery indicates that the observed effects are due to PYP photoactivation.

Length and Force Distributions of the pG State. The ΔL distributions for 36/128 PYP and 48/85 PYP (Fig. 4*a*) in the absence of illumination exhibit very different average values ($\pm$SE): 30.7 $\pm$ 0.8 and 12.1 $\pm$ 0.4 nm, respectively. These two values agree well with those expected based on the length differences between folded PYP ($\approx$3 nm) (6) and the amino acid contour length in fully unfolded PYP [assuming a distance of 0.38 nm (24) between two consecutive C^{α} in the protein backbone, 92 residues $\times$ 0.38 $\approx$ 35 nm in 36/128 PYP and 37 residues $\times$ 0.38 $\approx$ 14 nm in 48/85 PYP]. This agreement confirms the measurement of structural changes in the selected regions of the protein. Further analysis using the longest force–distance traces (with at least five rupture peaks) yield results identical to those from the entire data set (supporting information), providing quantitative validation of the polyprotein approach. This analysis excludes possible distortions of the AFM data by terminal PYP modules that could potentially give rise to a spurious unfolding length or force because of their random physical attachment to the AFM tip and the glass substrate surface. These findings confirm our measurement of structural changes in the selected regions of the protein.

The measured ΔF values for the two PYP mutants reveal significant anisotropy in the structural stability of PYP: ΔF is 86 $\pm$ 5 pN along the 36/128 axis and 66 $\pm$ 2 pN along the 48/85 axis (Fig. 5). In comparison, the unfolding force for two different pulling axes of ubiquitin were reported to be 203 vs. 85 pN (20) and 177 vs. <15 pN for the β-sheet protein E2lip3 (22).

Molecular Dynamics (MD) Simulation of Mechanical Anisotropy in the pG State. To further analyze the structural changes that occur in the pG state of PYP during these force–extension experiments, we performed steered MD (SMD) simulations of PYP. The distance between two residues in PYP corresponding to that used in the experiments was gradually increased by up to 5 nm by the application of an external force (25, 26). The simulations reveal very different unfolding pathways for the two pulling axes (Fig. 6). For the 36/128 axis, the overall structure of PYP initially remains essentially intact, which is reflected in the constant number of intramolecular hydrogen bonds in PYP as a function of pulling distance (Fig. 6) up to a distance of 1.2 nm. At this distance, an abrupt structural change occurs that disrupts all five hydrogen bonds between β-strand 1 and β-strand 6 and involves a concomitant sliding of these two strands with respect to each other. Extension beyond this rupture point results in a significant loss of structure in various regions of PYP. By contrast, pulling over the 48/85 axis of PYP is characterized by a gradual loss of structure and intramolecular hydrogen bonds in various regions of PYP as a function of pulling distance. Interestingly, the five hydrogen bonds between β-strand 1 and β-strand 6 remain intact up to an extension of at least 5 nm along this pulling axis. Thus, these simulations provide insight into the molecular structural basis for the two very different pathways of pG unfolding along the two pulling axes and into the structural changes that occur in the force–extension experiments.

Structural and Stability Changes Due to Photoactivation. To quantify the experimentally detected changes in PYP upon photoexcitation, we compared the force and length distributions detected during illumination of the sample to those for the pG state in the dark. Photoexcitation of PYP decreases the average unfolding force by $\approx$30%, from 66 $\pm$ 2 to 44 $\pm$ 1 pN for 48/85 PYP and from 86 $\pm$ 5 to 67 $\pm$ 2 pN for 36/128 PYP (Fig. 4), in line with destabilization of the light-activated pB state caused by its partial unfolding. In addition, photoexcitation decreases the length distributions (Fig. 4*b*) by 4 $\pm$ 1 nm in 36/128 PYP (from 30.7 $\pm$ 0.8 to 26.6 $\pm$ 0.7 nm) and by 2.9 $\pm$ 0.4 nm in 48/85 PYP (from 12.1 $\pm$ 0.4 to 9.2 $\pm$ 0.2 nm). The decrease in unfolding length corresponds to the length gained by PYP upon its photoconver-

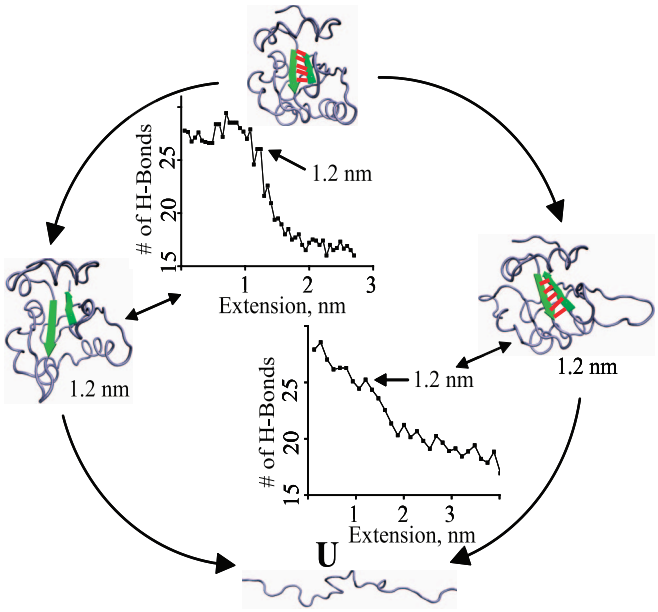

Fig. 6. SMD simulations of mechanical unfolding of the native pG state of PYP along the 36/128 axis (left half of cycle) and the 48/85 axis (right half of cycle) to reach the unfolded state (U, schematic). Two distinct pathways are found. The 36/128 pathway involves a well defined transition state (at a pulling distance of 1.2 nm) that is characterized by a sudden rupture of all five hydrogen bonds (in red) between two β-sheets (in green) in the center of the PAS core of pG. The 48/85 pathway involves gradual unfolding of the PAS core and successive rupturing of the H-bonds in the folded protein. The graphs show the total number of intraprotein H-bonds as a function of the pulling distance for the two pathways.

sion to the pB state (illustrated in Fig. 4*c*), and thus represents a 2-fold increase in the diameter of PYP. This large size increase should be interpreted by taking the finite sensitivity of the AFM cantilever into consideration. The instrument cannot resolve pulling events of less than the thermal noise level of 10 pN (peak-to-peak). Therefore, we conclude that light activation destabilizes portions of the PAS domain such that it is extensible by 3 nm with <10 pN of force. As an upper limit, the loss of protein stability would be $\approx 7\, k_BT$ [(10 pN × 3 nm)/k_BT; k_BT = 4 pN·nm]. The structural consequences of this expansion in the pB state can be obtained from the SMD extension simulations of the pG state. These simulations reveal a significant and global loss of structure (Fig. 4*c*) and a loss of approximately one-third of all intramolecular hydrogen bonds present in the native pG state for both pulling axes at an extension point corresponding to that experimentally detected for the pB state (Fig. 6). Thus, the experimental and computational results reported here demonstrate that light-triggered destabilization and partial unfolding of PYP occur in its core PAS domain, in contrast to the previous bulk solution measurements indicating unfolding of only the N-terminal α-helices of PYP (13–15).

Comparison with Other Experimental Data. The structural properties and stability of the pB state have been probed by a variety of bulk spectroscopic methods, allowing comparison with the single-molecule measurements reported here. Denaturant titration and stopped-flow rapid mixing experiments show that the stability of PYP is reduced from 42 kJ/mol in pG to 30 kJ/mol in pB (27, 28). The difference is in quantitative agreement with the reduced stability of the pB state observed in the single-molecule pulling experiments (17 kJ/mol $\approx 7\, k_BT$ for the upper limit of stability loss). A variety of experimental methods (10, 29, 30) show that the pB intermediate exhibits the thermodynamic properties of a partially unfolded state. H/D exchange monitored by NMR spectroscopy indicates that, although pB formation involves a significant loss of structure, it retains a well folded core (31). NMR measurements on a PYP derivative lacking the 25 N-terminal amino acids indicate that the central β-sheet in pB is still intact, whereas much of the remainder of the protein becomes highly flexible (16), implying an increase in the linear dimension of PYP of up to 4.5 Å along the two axes studied here. Small-angle x-ray scattering experiments on PYP and N-terminally truncated mutants revealed that the N-terminal 15 residues in PYP move away from the core of PYP upon pB formation, whereas the remainder of PYP swells by 0.7 Å (15). In summary, these data support the notion that pB is partially unfolded and has increased linear dimensions, in line with the single-molecule measurements described here. However, the extent of the increase in size detected in the AFM experiments is significantly larger. Our interpretation of this observation is that the bulk spectroscopic measurements probe the thermally averaged properties of pB as it fluctuates through a variety of conformations in this partially unfolded state. In contrast, the single-molecule pulling experiments probe the position of the energetic barrier for stability in pB (within the 10-pN noise limit) and, thus, report a maximally extended configuration to the edge of the energetic well that defines the pB state.

Conclusions

The mechanism of receptor activation is a central question in biological signal transduction and has been studied by a range of genetic, spectroscopic, and structural methods in various receptor systems. For this study, we used single-molecule force spectroscopy to probe receptor activation, allowing the detection of protein conformational changes during receptor activation at the single-molecule level. Our approach is to select a section of the protein by introducing Cys side chains at solvent-exposed positions, allowing the directed multimerization of the protein. Traditionally, the choice of the pulling axis in single-molecule manipulation experiments is limited, because polyproteins are constructed either by N-to-C linkage via genetic concatemerization (19) or by naturally occurring amino acid linkages (20). Yang *et al.* (23) used Cys-directed multimerization of T4 lysozymes in protein crystals. Applications of this crystal-assisted multimerization approach are limited because it requires protein crystallization and the use of Cys residues in sites that are adjacent in the crystal lattice.

The Cys-directed multimerization reaction in solution described here provides a powerful and general tool to study axis-dependent mechanical stability by using force spectroscopy measurements and to explore conformational changes during light- or ligand-induced protein function at the single-molecule level. Strategic Cys mutations can be engineered into the sequence to select a region of interest in the protein. This approach allows the identification of regions of PYP that undergo structural changes upon photoactivation, revealing the partial unfolding of its PAS domain. This result indicates that in addition to N- or C-terminal helices, the PAS domain itself can also undergo partial unfolding during signal transduction. Future AFM experiments on additional double-Cys PYP mutants will allow the mapping of structural changes to be extended to all regions of PYP. The two limitations to this approach are that the length increase between the two Cys residues and the mechanical stability along the chosen pulling axis should be above the distance (0.3 nm) and force (10 pN) detection limits of the AFM technique, respectively.

The emerging mechanism of receptor activation in PYP contains the following steps: (*i*) initial chromophore photoisomerization (32), which triggers (*ii*) active site proton transfer (33) that causes (*iii*) an electrostatically triggered protein quake (12), resulting in structural disruption of the PAS domain core,

which is relayed (*iv*) to the N-terminal helices (13, 14) by the side chain of Asn-43 (34). Future studies are needed to reveal how partial PAS domain unfolding contributes to signaling and whether this mechanism operates more widely in the PAS domain family.

Materials and Methods

Cys-Directed PYP Multimerization. An N-terminal histidine-tagged version of PYP from *Halorhodopsira halophila* was overproduced in *Escherichia coli* by using the pQE80 plasmid (Qiagen) and purified by Ni-affinity chromatography (33). To ensure maximal purity of the protein, the PYP sample bound to the Ni resin was washed extensively using three different washing buffers with the following order: (*i*) 50 mM $NaPO_4$/50 mM NaCl, pH 7.2; (*ii*) 50 mM $NaPO_4$/200 mM NaCl, pH 7.2; (*iii*) 50 mM $NaPO_4$/200 mM NaCl/2 mM imidazole, pH 7.2. Each washing buffer used at least three column volumes. Elution of PYP was performed with 50 mM $NaPO_4$/200 mM NaCl/100 mM imidazole, pH 7.2. The Cys mutants of PYP were obtained by mutagenic PCR using the QuikChange kit (Stratagene) and confirmed by DNA sequencing. Protein purification was performed in the absence of reducing agents. PYP mutants were concentrated to ≈5 mg/ml using Centricons (Millipore) and then injected into a dialysis cassette (Pierce, Rockford, IL). The multimerization reaction was carried out overnight in the presence of a constant stream of air bubbling through the solution in a buffer consisting of 50 mM $NaPO_4$ and 200 mM NaCl, pH 8.0. Exposure of the PYP mutants to air resulted in their spontaneous multimerization into polyPYP. The longest PYP multimers were selected by size exclusion chromatography in 50 mM $NaPO_4$/50 mM NaCl, pH 7.2, and concentrated in the same $NaPO_4$ buffer. The final PYP concentration of the polyPYP sample used for AFM experiments was ≈0.1–0.5 mg/ml.

Force Spectroscopy of Single polyPYP Molecules. New gold-coated, silicon nitrite AFM cantilevers (Bio-Levers; Olympus) were treated in a UV/Ozone cleaner (Novascan, Ames, IA) for 30 min and washed in chloroform. The spring constants (6.4 pN/nm and 22 pN/nm) of the two types of cantilevers used in the experiments were calibrated by applying the equipartition theorem to the thermal noise spectrum (35). A 100-μl drop of the polyPYP sample was applied to a clean glass slide. All data were collected using an AFM instrument (MFP-ID; Asylum Research, Santa Barbara, CA) on top of an inverted Nikon microscope. Light from a 452-nm blue laser (Melles–Griot, Carlsbad, CA) was focused with a ×10 objective to excite PYP at 1,000 mW/cm^2. UV/visual light absorbance measurements of polyPYP under identical conditions indicated that this light intensity results in nearly 100% photoconversion of the pG state to the pB state (supporting information). Only force–distance curves containing at least three consecutive rupture events were selected for analysis. The last rupture event was rejected because it usually represents detachment of the polyPYP molecule from the glass surface or tip of the cantilever. The short distance between rupture events in 48/85 PYP does not allow reliable worm-like chain analysis. Hence, the unfolding lengths for 48/85 and 36/128 data were analyzed in the same manner by measuring the distances between consecutive dips in the force–extension curves. Measuring the distances between consecutive peaks yielded similar unfolding length distributions.

SMD Simulations. SMD simulations (25) of PYP were performed with the NAMD program (26) and the CHARMM27 (36) force field. The structure of PYP (Protein Data Bank ID code 2PHY) was solvated and equilibrated in water at 300 K for 1 ns. We simulated the single PYP stretching by fixing the C^α of residue 48 (or 36) and applying external forces to the C^α of residue 85 (or 125). We applied the forces by restraining residue 85 (or 125) to a harmonic potential and moving at a constant velocity in the direction connecting 48–85 (or 36–125). PYP was stretched at 0.1 Å/ps for 1 ns. We repeated the simulations three times along the 48/85 and 36/125 axes and obtained similar results.

We thank Jennifer Miller for help with MD simulations and Philippe Cluzel and Tobin Sosnick for stimulating discussions. J.M.Z. was supported by National Institutes of Health Grant GM008720 and Burroughs Wellcome Fund Interfaces Grant 1001774. R.A.N. was supported by a Coordenação de Aperfeiçoamento de Pessoal de Nível Superior of Brazil graduate research fellowship. W.D.H. was supported by National Institutes of Health Grant GM063805. N.F.S. was partially supported by a seed grant from the University of Chicago Institute for Biophysical Dynamics and by National Science Foundation–Materials Research Science and Engineering Centers Grant DMR 0213745.

1. Taylor, B. L. & Zhulin, I. B. (1999) *Microbiol. Mol. Biol. Rev.* **63,** 479–506.
2. Vincent, G. M. (1998) *Annu. Rev. Med.* **49,** 263–274.
3. Semenzal, G. L. (2000) *Genes Dev.* **14,** 1983–1991.
4. Pellequer, J.-L., Wagner-Smith, K. A., Kay, S. A. & Getzoff, E. D. (1998) *Proc. Natl. Acad. Sci. USA* **95,** 5884–5890.
5. Hefti, M. H., Francoijs, K. J., de Vries, S. C., Dixon, R. & Vervoort, J. (2004) *Eur. J. Biochem.* **271,** 1198–1208.
6. Borgstahl, G. E. O., Williams, D. R. & Getzoff, E. D. (1995) *Biochemistry* **34,** 6278–6287.
7. Hoff, W. D., Dux, P., Hård, K., Devreese, B., Nugteren-Roodzant, I. M., Crielaard, W., Boelens, R., Kaptein, R., van Beeumen, J. & Hellingwerf, K. J. (1994) *Biochemistry* **33,** 13959–13962.
8. Meyer, T. E., Yakali, E., Cusanovich, M. A. & Tollin, G. (1987) *Biochemistry* **26,** 418–423.
9. Sprenger, W. W., Hoff, W. D., Armitage, J. P. & Hellingwerf, K. J. (1993) *J. Bacteriol.* **175,** 3096–3104.
10. Lee, B. C., Pandit, A., Croonquist, P. A. & Hoff, W. D. (2001) *Proc. Natl. Acad. Sci. USA* **98,** 9062–9067.
11. Genick, U. K., Borgstahl, G. E., Ng, K., Ren, Z., Pradervand, C., Burke, P. M., Srajer, V., Teng, T. Y., Schildkamp, W., McRee, D. E., *et al.* (1997) *Science* **275,** 1471–1475.
12. Xie, A., Kelemen, L., Hendriks, J., White, B. J., Hellingwerf, K. J. & Hoff, W. D. (2001) *Biochemistry* **40,** 1510–1517.
13. Harigai, M., Imamoto, Y., Kamikubo, H., Yamazaki, Y. & Kataoka, M. (2003) *Biochemistry* **42,** 13893–13900.
14. van der Horst, M. A., van Stokkum, I. H. M., Crielaard, W. & Hellingwerf, K. J. (2001) *FEBS Lett.* **497,** 26–30.
15. Imamoto, Y., Kamikubo, H., Harigai, M., Shimizu, N. & Kataoka, M. (2002) *Biochemistry* **41,** 13595–13601.
16. Bernard, C., Houben, K., Derix, N. M., Marks, D., van der Horst, M. A., Hellingwerf, K. J., Boelens, R., Kaptein, R. & van Nuland, N. A. (2005) *Structure (London)* **13,** 953–962.
17. Harper, S. M., Neil, L. C. & Gardner, K. H. (2003) *Science* **301,** 1541–1544.
18. Bustamante, C., Macosko, J. C. & Wuite, G. J. L. (2000) *Nat. Rev. Mol. Cell. Biol.* **1,** 130–136.
19. Carrion-Vazquez, M., Oberhauser, A. F., Fisher, T. E., Marszalek, P. M., Li, H. & Fernandez, J. M. (2001) *Prog. Biophys. Mol. Biol.* **74,** 63–91.
20. Carrion-Vazques, M., Li, H., Lu, H., Marszalek, P. E., Oberhauser, A. F. & Fernandez, J. M. (2003) *Nat. Struct. Biol.* **10,** 738–743.
21. Dietz, H. & Rief, M. (2006) *Proc. Natl. Acad. Sci. USA* **103,** 1244–1247.
22. Brockwell, D. J., Paci, E., Zinober, R. C., Beddard, G. S., Olmsted, P. D., Smith, D. A., Perham, R. N. & Radford, S. E. (2003) *Nat. Struct. Biol.* **10,** 731–737.
23. Yang, G., Cecconi, C., Baase, W. A., Vetter, I. R., Breyer, W. A., Haack, J. A., Matthews, B. W., Dahlquist, F. W. & Bustamante, C. (2000) *Proc. Natl. Acad. Sci. USA* **97,** 139–144.
24. Fisher, T. E., Oberhauser, A. F., Carrion-Vazquez, M., Marszalek, P. E. & Fernandez, J. M. (1999) *Trends Biochem. Sci.* **24,** 379–384.
25. Lu, H. & Schulten, K. (1999) *Protein Struct. Funct. Genet.* **45,** 453–463.
26. Nelson, M. T., Humphrey, W., Gursoy, A., Dalke, A., Kale, L. V., Steel, R. D. & Schulten, K. (1996) *Int. J. Supercomput. Appl. High Perform. Comput.* **10,** 251–268.
27. Lee, B. C., Croonquist, P. A., Sosnick, T. R. & Hoff, W. D. (2001) *J. Biol. Chem.* **276,** 20821–20823.
28. Ohishi, S., Shimizu, N., Mihara, K., Imamoto, Y. & Kataoka, M. (2001) *Biochemistry* **40,** 2854–2859.
29. van Brederode, M. E., Hoff, W. D., van Stokkum, I. H. M., Groot, M. L. & Hellingwerf, K. J. (1996) *Biophys. J.* **71,** 365–380.

30. Takeshita, K., Imamoto, Y., Kataoka, M., Tokunaga, F. & Terazima, M. (2002) *Biochemistry* **41,** 3037–3048.
31. Craven, C. J., Derix, N. M., Hendriks, J., Boelens, R., Hellingwerf, K. J. & Kaptein, R. (2000) *Biochemistry* **39,** 14392–14399.
32. Kort, R., Vonk, H., Xu, X., Hoff, W. D., Crielaard, W. & Hellingwerf, K. J. (1996) *FEBS Lett.* **382,** 73–78.
33. Xie, A., Hoff, W. D., Kroon, A. R. & Hellingwerf, K. J. (1996) *Biochemistry* **35,** 14671–14678.
34. Rajagopal, S., Anderson, S., Srajer, V., Schmidt, M., Pahl, R. & Moffat, K. (2005) *Structure (London)* **13,** 55–63.
35. Hutter, J. L. & Bechhoefer, J. (1993) *Rev. Sci. Instrum.* **64,** 1868–1873.
36. MacKerell, A. D. (1998) *J. Phys. Chem.* **102,** 3586–3616.